

Magneto-convective non-Newtonian nanofluid with momentum and temperature dependent slip flow from a permeable stretching sheet with porous medium and chemical reaction

T. Prasanna kumar¹ and K. Gangadhar²

^{1,2}Department of Mathematics, Acharya Nagarjuna University, Ongole, Andhra Pradesh -523001, India

Abstract: The two-dimensional magnetohydrodynamic boundary layer flow of non-Newtonian power-law nanofluids past a porous stretching sheet with linear hydrodynamic slip boundary condition in the presence of chemical reaction and temperature dependent slip boundary condition. Using the similarity transformations, the governing equations have been transformed into a system of ordinary differential equations. These differential equations are highly nonlinear which cannot be solved analytically. Therefore, bvp4c MATLAB solver has been used for solving it. Numerical results are obtained for the skin-friction coefficient, the local Nusselt number and the local Sherwood number as well as the velocity, temperature and Concentration profiles for different values of the governing parameters, namely, the power-law index parameter, Lewis number, Prandtl number, thermophoresis parameter, Brownian motion parameter, magnetic field parameter, linear momentum slip parameter, permeability parameter, temperature dependent slip parameter and chemical reaction parameter.

Keywords: Non-Newtonian nanofluids, MHD flow, Hydrodynamic slip, linear group transformations, porous medium, temperature dependent slip flow, chemical reaction.

I. Introduction

Nanoparticles range in diameter between 1 and 100 nm. Nanofluids commonly contain up to a 5% volume fraction of nanoparticles to ensure effective heat transfer enhancements. One of the main objectives of using nanofluids is to achieve the best thermal properties with the least possible (<1%) volume fraction of nanoparticles in the base fluid. The term nanofluid was first proposed by Choi [1] to indicate engineered colloids composed of nanoparticles dispersed in a base fluid. The characteristic feature of nanofluids is thermal conductivity enhancement; a phenomenon observed by Masuda et al. [2].

Study of non-Newtonian fluids over a stretching surface achieved great attention due to its large number of application. In fact, the effects of non-Newtonian behavior can be determined due to its elasticity, but sometimes rheological properties of fluid are identified by their constitutive equations. In view of rheological parameters, the constitutive equations in the non-Newtonian fluids are more complex and thus give rise the equations which are complicated than the Navier–Stokes equations. Many of the fluids used in the oil industry and simulate reservoirs are significantly non-Newtonian. In different degree, they display shear-dependent of viscosity, thixotropy and elasticity (Pearson and Tardy [3]; Ellahi and Afza [4]; Ellahi [5]). Gorla and Kumari [6] studied the mixed convection flow of a non-newtonian nanofluid over a non-linearly stretching sheet.

The no-slip boundary condition is known as the central tenets of the Navier–Stokes theory. However, there are situations wherein such a condition is not appropriate. The fluids exhibiting boundary slip find applications in technology such as in the polishing of artificial heart valves and internal cavities. Recently, micro-scale fluid dynamics in micro-electromechanical systems (MEMS) received much attention. In all the aforementioned investigations, the no-slip condition at the boundary has been assumed. The non-adherence of the fluid to a solid boundary, also known as velocity slip, is a phenomenon that has been observed in certain circumstances. Even in literature, there is a scarcity of the study of the slip flow over a flat plate. Crane [7] pioneered the study of stretching sheet by presenting an exact analytical solution for the steady two-dimensional stretching of a plate in a quiescent fluid. Since then, many authors have considered various aspects of this problem. Wang [8] extended Crane's study to include both suction and slip effects at the boundary.

Owing to numerous industrial and engineering applications, the MHD flow analysis of the nanofluids (mixture of fluids and nanoparticles) has been increased in recent years. Qasim et al. [9] investigates the magnetohydrodynamic (MHD) flow of ferrofluid along a stretching cylinder. El-Gaied and Hamad [10] was found that alumina nanoparticles when suspended in a fluid are capable of increasing the heat transfer capability of the base fluid and conclude that the shear stress as well as heat transfer rate increases with nanoparticle volume fraction. Nandy and Mahapatra [11] analyzed the effects of velocity slip and heat generation/absorption on magnetohydrodynamic (MHD) stagnation-point flow and heat transfer over a stretching/shrinking surface, with convective boundary conditions, in the presence of nanoparticle fractions. Eldabe et al. [12] analyzed the effects of magnetic field and heat generation on viscous flow and heat transfer over a nonlinearly stretching

surface in a nanofluid. Bhattacharyya et al. [13] conclude that the increase of magnetic and slip parameters reduce the boundary layer thickness and also enhance the heat transfer from the plate. Santosh Chaudhary and Pradeep Kumar [14] studied the steady two-dimensional laminar boundary layer flow of a viscous, incompressible, electrically conducting fluid near a stagnation point past a shrinking sheet with slip in the presence of a magnetic field. Uddin et al. [15] reported that increasing thermophoresis parameter boosts both the temperatures and nanoparticle concentration magnitudes throughout the boundary layer regime.

In many engineering problems, the thermal conductivity is reported as a function of the temperature as the value of thermal conductivity changes with temperature especially if the region of temperature change is large (Mierzwiczak & Kolodzie [16]). Some recent papers that considered the temperature-dependent thermal conductivity includes Abel et al. [17] who studied the flow of a power-law fluid past a vertical stretching sheet and Ahmad et al. [18] who studied the boundary layer flow of viscous incompressible fluid over a stretching plate. According to Shang [19], the effect of variable thermal conductivity on heat transfer coefficient is greater than the variable absolute viscosity. Mierzwiczak and Kołodzie [16] studied the non-iterative inverse determination of temperature-dependent thermal conductivity in two-dimensional steady-state heat conduction problem. They modeled the thermal conductivity in the form of a polynomial function of temperature with unknown coefficients. Mutlag et al. [20] conclude that the dimensionless temperature decreases when thermal conductivity increases.

The present study investigates the two-dimensional magnetohydrodynamic boundary layer flow of non-Newtonian power-law nanofluids past a porous stretching sheet with linear hydrodynamic slip boundary condition in the presence of chemical reaction and temperature dependent slip boundary condition. Using the similarity transformations, the governing equations have been transformed into a set of ordinary differential equations, which are nonlinear and cannot be solved analytically, therefore, bvp4c MATLAB solver has been used for solving it. The results for velocity, temperature and concentration functions are carried out for the wide range of important parameters namely; magnetic parameter, permeability parameter, thermal conductivity parameter, velocity slip parameter, thermophoresis parameter, Brownian motion parameter and chemical reaction parameter. The skin frictions, the rate of heat and mass transfer have also been computed.

II. Mathematical Formulation

Consider the two-dimensional (\bar{x}, \bar{y}) steady-state MHD boundary layer slip flow of an electrically-conducting and chemically reacting non-Newtonian power law nanofluid from a heated porous stretching sheet. The nanofluid is assumed to be single phase, in thermal equilibrium and there is a slip velocity and thermal slip flow between base fluid and particles. The nanoparticles are assumed to have uniform shape and size. Thermophysical properties are assumed to be invariant. A transverse magnetic field of constant strength is imposed in the \bar{y} direction. Hall current and Alfvén wave effects are neglected as are magnetic induction and Ohmic dissipation. The sheet surface is also assumed to be non-conducting. The governing flow field equations in dimensional form are obtained by combining the models of Andersson and Bech [21] and Makinde and Aziz [22]:

Continuity equation

$$\frac{\partial \bar{u}}{\partial \bar{x}} + \frac{\partial \bar{v}}{\partial \bar{y}} = 0 \tag{2.1}$$

Linear momentum equation

$$\bar{u} \frac{\partial \bar{u}}{\partial \bar{x}} + \bar{v} \frac{\partial \bar{u}}{\partial \bar{y}} = -\frac{K}{\rho} \frac{\partial}{\partial \bar{y}} \left(-\frac{\partial \bar{u}}{\partial \bar{y}} \right)^n - \frac{\sigma B_0^2}{\rho} \bar{u} - \frac{\nu}{k} \bar{u} \tag{2.2}$$

Energy equation

$$\bar{u} \frac{\partial T}{\partial \bar{x}} + \bar{v} \frac{\partial T}{\partial \bar{y}} = \alpha \frac{\partial^2 T}{\partial \bar{y}^2} + \tau D_B \frac{\partial T}{\partial \bar{y}} \frac{\partial C}{\partial \bar{y}} + \tau \left(\frac{D_T}{T_\infty} \right) \left(\frac{\partial T}{\partial \bar{y}} \right)^2 \tag{2.3}$$

$$\bar{u} \frac{\partial C}{\partial \bar{x}} + \bar{v} \frac{\partial C}{\partial \bar{y}} = D_B \frac{\partial^2 C}{\partial \bar{y}^2} + \left(\frac{D_T}{T_\infty} \right) \frac{\partial^2 T}{\partial \bar{y}^2} - k_1 (C - C_\infty) \tag{2.4}$$

Where \bar{u} and \bar{v} are the velocity components in the \bar{x} - and \bar{y} - directions, respectively, $\alpha = \frac{k}{(\rho c_p)}$ is the

thermal diffusivity of the fluid and $\tau = \frac{(\rho c)_p}{(\rho c)_f}$ is the ratio of heat capacities, and all other terms are defined in

the notation section. The boundary conditions at the wall (sheet) and in the free stream are prescribed thus:

The boundary conditions are

$$\begin{aligned} \bar{u} = \bar{u}_w + \bar{u}_{slip} = U_r \left(\frac{\bar{x}}{L} \right) + N_1 v \left(-\frac{\partial \bar{u}}{\partial \bar{y}} \right)^{n-1} \left(\frac{\partial \bar{u}}{\partial \bar{y}} \right), \bar{v} = \bar{v}(\bar{x}), T = T_w + D_1(\bar{x}) \frac{\partial T}{\partial \bar{y}}, C = C_w \quad \text{at } \bar{y} = 0 \\ \bar{u} \rightarrow 0, T \rightarrow T_\infty, C \rightarrow C_\infty \quad \text{as } \bar{y} \rightarrow \infty \end{aligned} \quad (2.5)$$

Here U_r is a reference velocity, L is the characteristic of length, and N_1 is the slip factor having the dimension (seconds/metres). It needs to be mentioned that for the non-Newtonian power law model, the case of $N < 1$ is associated with shear-thinning fluids (pseudo plastic fluids), $D_1(x)$ is the thermal variable slip factor with dimensional length, $n = 1$ corresponds to Newtonian fluids and $n > 1$ applies to the case of shear-thickening (dilatants), k_1 is the chemical reaction constant.

We now introduce the following dimensionless variables to reduce the number of independent variables and the number of equations,

$$x = \frac{\bar{x}}{L}, y = \frac{\bar{y} \text{Re}_L^{n+1}}{L}, u = \frac{\bar{u}}{U_r}, v = \frac{\bar{v} \text{Re}_L^{n+1}}{U_r}, \theta = \frac{T - T_\infty}{T_w - T_\infty}, \phi = \frac{C - C_\infty}{C_w - C_\infty} \quad (2.6)$$

Here Re is the Reynolds number

We introduce also a stream functions ψ is defined by

$$u = \frac{\partial \psi}{\partial y}, v = -\frac{\partial \psi}{\partial x} \quad (2.7)$$

The normalized transformed partial differential conservation equations are thereby reduced to

The dimensionless forms of the governing equations

$$\frac{\partial \psi}{\partial y} \frac{\partial^2 \psi}{\partial x \partial y} - \frac{\partial \psi}{\partial x} \frac{\partial^2 \psi}{\partial y^2} - n \left(-\frac{\partial^2 \psi}{\partial y^2} \right)^{n-1} \frac{\partial^2 \psi}{\partial y^3} + (M + K) \frac{\partial \psi}{\partial y} = 0 \quad (2.8)$$

$$\frac{\partial \psi}{\partial y} \frac{\partial \theta}{\partial x} - \frac{\partial \psi}{\partial y} \frac{\partial \theta}{\partial y} - \frac{1}{\text{Pr}} \frac{\partial^2 \theta}{\partial y^2} - \text{Nb} \frac{\partial \theta}{\partial y} \frac{\partial \phi}{\partial y} - \text{Nt} \left(\frac{\partial \theta}{\partial y} \right)^2 = 0 \quad (2.9)$$

$$\frac{\partial \psi}{\partial y} \frac{\partial \phi}{\partial x} - \frac{\partial \psi}{\partial x} \frac{\partial \phi}{\partial y} - \frac{1}{\text{Le}} \frac{\partial^2 \phi}{\partial y^2} - \frac{1}{\text{Le}} \frac{\text{Nt}}{\text{Nb}} \frac{\partial^2 \theta}{\partial y^2} - \text{kr} \phi = 0 \quad (2.10)$$

here $M = \frac{\sigma B_0^2 L}{\rho U_r}$ is the magnetic body force parameter, $\text{Re}_L = \frac{\rho L^n U_r^{2-n}}{K}$ is the uniform Reynolds number,

$\text{Pr}_L = \frac{U_r L}{\alpha} \left(\frac{\rho L^n U_r^{2-n}}{k} \right)^{\frac{2}{n+1}}$ is the uniform Prandtl number, $K = \frac{\nu L}{k U_r}$ the permeability parameter,

$\text{Nb}_L = \tau D_B \Delta C \left(\frac{U_r^{\frac{3-3n}{2}} L^{\frac{n-1}{2}} \rho}{K} \right)$ is the uniform Brownian motion parameter, $\text{Nt}_L = \frac{\tau D_T \Delta T}{T_\infty} \left(\frac{U_r^{\frac{3-3n}{2}} \rho}{K} \right)$ is

the uniform thermophoresis parameter, $Le_L = \frac{LU_r}{D_B} \left(\frac{\rho L^n U_r^{2-n}}{K} \right)^{\frac{2}{n+1}}$ is the uniform Lewis number and

$fW_L = \frac{v_w \text{Re}_L^{\frac{1}{n+1}}}{U_r}$ is the uniform suction parameter.

The boundary conditions become,

$$\frac{\partial \psi}{\partial y} = x + \frac{N_1 v}{L^n} U_r^{n-1} \text{Re}_L^{\frac{n}{n+1}} \left(-\frac{\partial^2 \psi}{\partial y^2} \right)^{n-1} \left(\frac{\partial^2 \psi}{\partial y^2} \right), \frac{\partial \psi}{\partial x} = fW_L, \theta = 1 + \frac{D_1 \text{Re}_L^{\frac{1}{n+1}}}{L} \frac{\partial \theta}{\partial y}, \phi = 1 \text{ at } y = 0$$

$$\frac{\partial \psi}{\partial y} = \theta = \phi = 0 \quad \text{as } y \rightarrow \infty \tag{2.11}$$

we transform this system to an ordinary system using scaling group transformations,

$$\Gamma : x^* = xA^{\alpha_1}, y^* = yA^{\alpha_2}, \psi^* = \psi A^{\alpha_3}, \theta^* = \theta A^{\alpha_4}, \phi^* = \phi A^{\alpha_5} \tag{2.12}$$

where $A(\alpha_i, i = 1, 2, 3, \dots, 5)$ are all arbitrary real constants. We seek the values of α_i such that the form of Eqs. (2.8)-(2.11) is invariant under the transformations in (2.12). Substituting new variables in Eq. (2.12) into Eqs. (2.8)-(2.11), equating powers of A (to confirm the invariance of the Eqs. (2.8)-(2.11) under this group of transformations), we have, following Hansen [23] and Shang [24]:

$$2\alpha_3 - 2\alpha_2 - \alpha_1 = (n-1)\alpha_3 - 2(n-1)\alpha_2 + \alpha_3 - 3\alpha_2 = \alpha_3 - \alpha_2$$

$$\alpha_4 + \alpha_3 - \alpha_2 - \alpha_1 = \alpha_4 - 2\alpha_2 = \alpha_4 + \alpha_5 - 2\alpha_2 = 2\alpha_4 - 2\alpha_2$$

$$\alpha_4 + \alpha_3 - \alpha_2 - \alpha_1 = \alpha_5 - 2\alpha_2 = \alpha_4 - 2\alpha_2 = \alpha_5 \tag{2.13}$$

Solving the linear system defined by Eq. (2.13), we arrive indue course at:

$$\alpha_1 = \frac{n+1}{2n} \alpha_3, \alpha_2 = \frac{n-1}{2n} \alpha_3, \alpha_4 = \alpha_5 = 0 \tag{2.14}$$

Here at least one of $\alpha_i \neq 0$ ($i = 1, 2, 3, 4, 5$)-if all $\alpha_i = 0$, this group method is invalidated, as further elaborated by Hansen [23]. Next, we seek ‘‘absolute invariants’’ under this elected group of transformations. Absolute invariants are the functions possessing the same form before and after the transformation. It is apparent from Eqs. (2.12) and (2.14) that:

$$\frac{y}{x^{\frac{n-1}{2n}}} = \frac{y^*}{x^{*2n}} \tag{2.15}$$

This combination of variables is therefore invariant under the present group of transformations and consequently, it constitutes an absolute invariant. We denote this functional form by:

$$\eta = \frac{y}{x^{\frac{n-1}{2n}}} = \frac{y^*}{x^{*2n}} \tag{2.16}$$

By the same argument, other absolute invariants are readily yielded:

$$\psi = x^{\frac{2n}{n+1}} f(\eta), \theta = \theta(\eta), \phi = \phi(\eta) \tag{2.17}$$

Here η is the similarity independent variable, $f(\eta), \theta(\eta), \phi(\eta)$ are the dimensionless stream function, temperature and nanoparticle concentration functions, respectively. Using Eqs. (2.16) and (2.17), it emerges that Eqs. (2.8)-(2.11) may be written as the following ‘‘local similarity’’ ordinary differential equations:

$$n(-f'')^{n-1} f''' + \frac{2n}{n+1} f f'' - f'^2 - (M + K) f' = 0 \tag{2.18}$$

$$\frac{1}{\text{Pr}_x} \theta'' + Nb_x \theta' \phi' + Nt_x \theta'^2 + \frac{2n}{n+1} f \theta' = 0 \tag{2.19}$$

$$\frac{1}{Le_x} \phi'' + \frac{1}{Le_x} \frac{Nt_x}{Nb_x} \theta'' + \frac{2n}{n+1} f \phi' - kr \phi = 0 \tag{2.20}$$

The corresponding boundary conditions are

$$\begin{aligned} f'(0) &= 1 + a_x \left[-f''(0) \right]^{n-1} f''(0), f(0) = fw_x, \theta(0) = 1 + b_x \theta'(0), \phi(0) = 1 \\ f'(\infty) &= \theta(\infty) = \phi(\infty) = 0 \end{aligned} \tag{2.21}$$

Here $Pr_x = Pr_L x^{\frac{2n-2}{n+1}}$ is the local Prandtl number, $Nb_x = Nb_L x^{\frac{2n-2}{n+1}}$ is the local Brownian motion parameter, $Nt_x = Nt_L x^{\frac{2n-2}{n+1}}$ is the local thermophoresis parameter, $Le_x = Le_L x^{\frac{2n-2}{n+1}}$ is the local Lewis number, $a_x = \frac{N_1 \nu}{L^n} U_r^{n-1} Re_L^{\frac{n}{n+1}} x^{\frac{n-1}{n+1}}$ is the local momentum slip parameter, $fw_x = fw_L x^{\frac{2n-2}{n+1}}$ is the local

lateral mass flux (wall suction/injection) parameter and $b_x = D_1 \frac{Re_x^{\frac{1}{n-1}}}{Lx^{2n}}$ thermal slip parameter. In adopting

local similarity solutions, we have deployed a subscript x. This subscript (.x) is now dropped for brevity when referring to the local dimensionless numbers hereafter.

It is interesting to note that the transformed local similarity model developed reduces exactly to the Newtonian nanofluid transport model of Makinde and Aziz [22] and also to that of Noghrebadi et al. [25] for $n=1$ (Newtonian fluids), $M=0$ (vanishing magnetic field), $fw=0$ (solid wall, i.e., suction/injection absent) and no wall momentum slip. ($a=0$) Furthermore the current model retracts to that of Andersson and Bech [21] for the impermeable wall case ($fw=0$) with nanofluid characteristics neglected (i.e., Eq. (2.20) dropped and $Nb=Nt=0$) and with no wall slip ($a=0$) Finally the model presented by Xu and Liao [26] is retrieved in absence of magnetohydrodynamic, species diffusion (nanoparticle) and momentum slip effects, Finally Uddin et al. [15] developed in the absence of porous medium, chemical reaction, temperature dependent slip flow effects. These cases therefore provide excellent benchmarks for validating the numerical solutions developed for the present more general boundary value problem.

Expressions for the quantities of physical interests, the skin friction factor and the rate of heat and mass transfer can be found from the following definitions:

$$C_{f_x} = \frac{2K}{\rho u_w^{-2}} \left(\frac{\partial \bar{u}}{\partial y} \right)_{y=0}, Nu_x = \frac{-\bar{x}}{T_w - T_\infty} \left(\frac{\partial T}{\partial y} \right)_{y=0}, Sh_x = \frac{-\bar{x}}{C_w - C_\infty} \left(\frac{\partial C}{\partial y} \right)_{y=0} \tag{2.21}$$

Using (2.6) and (2.21) into (2.25) we get,

$$Re_x^{\frac{1}{n+1}} C_{f_x} = 2 \left[f''(0) \right]^n, Re_x^{\frac{1}{n+1}} Nu_x = -\theta'(0), Re_x^{\frac{1}{n+1}} Sh_x = -\phi'(0) \tag{2.22}$$

where $Re_x = \frac{u_w x}{\nu}$ is the local Reynolds number. It is pertinent to highlight that the local skin friction factor, local Nusselt number and local Sherwood number are directly proportional to the numerical values of $[-2f''(0)]^n, -\theta'(0)$ and $-\phi'(0)$ respectively. In the parlance of Kuznetsov and Nield [27], $Nu_x Re_x^{\frac{1}{n+1}}$ and $Sh_x Re_x^{\frac{1}{n+1}}$ may be referred as the reduced local Nusselt number, Nu_r , and reduced local Sherwood number, Sh_r , for non-Newtonian nanofluids, and are represented by $-\theta'(0)$ and $-\phi'(0)$, respectively.

III. Solution Of The Problem

The set of equations (2.12) to (2.24) were reduced to a system of first-order differential equations and solved using a MATLAB boundary value problem solver called **bvp4c**. This program solves boundary value problems for ordinary differential equations of the form $y' = f(x, y, p), a \leq x \leq b$, by implementing a collocation method subject to general nonlinear, two-point boundary conditions $g(y(a), y(b), p)$. Here p is a vector of unknown parameters. Boundary value problems (BVPs) arise in most diverse forms. Just about any BVP can be formulated for solution with **bvp4c**. The first step is to write the ODEs as a system of first order ordinary differential equations. The details of the solution method are presented in Shampine and Kierzenka[28].

IV. Results And Discussion

Prior to describing full numerical solutions to the present problem, we validate the bvp4c MATLAB solver selected comparisons with previous studies. We compare the value of $-f''(0)$ with asymptotic solutions of Andersson and Bech [21], homotopy solutions of Xu and Laio [26], and Runge–Kutta–Fehlberg fourth fifth order numerical method in the symbolic computer software Maple 14 of Uddin et al [15] for non-Newtonian fluid in Table 1. Table 2 shows comparison of $-f''(0)$ for various magnetic parameters (M) and rheological power-law index (n) again with Andersson and Bech [21] and Uddin et al. [15]. The numerical results for $-\theta'(0)$ computed by bvp4cMATLAB solver are additionally benchmarked with those reported by Grubka and Bobba [29], Chen [30], Ishak [31]] and Uddin et al. [15] for Newtonian fluids, as presented in Table 3. In all cases we have found very close agreement is achieved and thus great confidence is assured in the accuracy of the bvp4c Matlab solver numerical results to be reported subsequently.

Figures 1-21 document the graphical computations for non-Newtonian power-law nanofluid flow characteristics, i.e., dimensionless axial velocity, temperature and nanoparticle concentration for the effects of the dictating thermophysical parameters. Figure 1-3 depict the influence of linear momentum slip (a), mass transfer velocity (f_w), thermal slip parameter (b), permeability parameter (K), magnetic field (M) and chemical reaction parameter (kr) on velocity profiles with transverse coordinate (η) for the pseudoplastic cases ($n = 0.5$) and also $n = 1$ (Newtonian fluids).

Inspection of Fig. 1-4, indicates that the velocity profiles are larger for a pseudoplastic fluid than for Newtonian fluid. Evidently with lower rheological index (n), the viscosity of the nanofluid is depressed and the boundary layer flow is accelerated. Since dilatant fluids are relatively rarely encountered in materials processing, the case of $n > 1$ is not examined here. Velocity is also found to decrease with increasing parameter momentum slip (Fig. 1), wall mass flux (Fig. 2), magnetic parameter (Fig. 3) and permeability parameter (Fig. 4). Increased momentum slip (Fig. 1) imparts a retarding effect to the flow at the wall and this influences the entire flow through the boundary layer, transverse to the wall. With increased mass flux into the sheet regime via the wall ($S < 0$, i.e., injection), the boundary layer flow is significantly accelerated, as observed in Fig. 2. The converse behaviour accompanies increasing mass flux out of the boundary layer ($S > 0$, i.e., suction). Evidently the suction effect induces greater adherence to the wall of the fluid regime and this also increases momentum boundary layer thickness. With greater injection, the momentum boost results in a reduction in momentum boundary layer thickness. These computations concur with many previous studies in transpiring boundary layer flows of nanofluids (Rana et al. [34]; Ferdows et al. [35]; Uddin et al [15]). The case of the impervious sheet, i.e., solid wall ($S = 0$) naturally falls between the injection and suction cases. With an increase in magnetic parameter, there is an escalation in magnitude of the Lorentzian hydromagnetic drag force. This very clearly acts to depress velocity magnitudes (Fig. 3) and even though the magnetic body force is only a linear term [$-Mf'$ in Eq. (2.18)] it exerts a very dramatic effect on the flow. Hydrodynamic (momentum) boundary layer thickness is therefore sizeably decreased with increasing values of M and same results were found with the influence of permeability parameter. In all four Fig. 1-4, asymptotically smooth convergence of computations is achieved into the free stream.

Figs. 5-7 present the response of temperature profiles, again for both pseudoplastic ($n=0.5$) and Newtonian ($n=1$) fluids, for a variation in momentum slip, wall mass flux. Temperatures are markedly elevated with pseudoplastic fluids compared with Newtonian fluids. Increasing momentum slip significantly increases the temperature magnitudes throughout the boundary layer regime and therefore enhances thermal boundary layer thickness (fig.5). These results are similar to the findings by Uddin et al. [15] in the absence of porous medium ($K=0$), temperature dependent slip flow ($b=0$) and chemical reaction ($kr=0$). The presence of injection ($S < 0$) as elaborated earlier, aids momentum development, i.e., viscous diffusion. This will also serve to encourage thermal diffusion leading to manifestly higher temperatures than for the suction case ($S > 0$) which will depress temperatures (Fig. 6). Injection therefore elevates thermal boundary layer thickness whereas suction decreases it. A similar observation has been reported by Makinde and Aziz [22], Rana et al. [32] and Uddin et al [15], who have also noted, as in the present case, that despite the strong influence of suction in decelerating the flow (and the corresponding cooling of the boundary layer), there is never any flow reversal (velocities are sustained as positive). The Lorentz force magnetohydrodynamic drag generated by the imposition of transverse magnetic field has the tendency to not only slow down the flow but achieves this at the expense of increasing temperature (Fig. 7). The supplementary kinetic energy necessary for dragging the magnetic nanofluid against the action of the magnetic field, even at relatively low values of magnetic field, is dissipated as thermal energy in the boundary layer. As elucidated by Be'g et al. [33] this is characteristic of boundary layer hydromagnetics and reproduces the famous ‘‘Rossow results’’. The overall effect is to boost the temperature. Clearly for the non-conducting case, temperatures will be minimized as magnetic field will vanish. Moreover for the pseudoplastic nanofluid case, temperatures are the highest achieved with the infliction of a magnetic field, and evidently this is beneficial in the synthesis of electro-conductive nanopolymers, as highlighted in the recent

theoretical studies by Rana et al. [34], Ferdows et al. [36], and further emphasized in the experimental study of Crainic et al. [37]. Figure 8-10 depict the evolution of temperature fields with a variation in thermophoresis number (Nt), Brownian motion parameter (Nb) and Prandtl number (Pr), respectively, in all cases for both Newtonian and pseudoplastic nanofluids. A consistent response is not observed in all the temperature profiles with rheological index, as computed in earlier graphs. In Fig. 8, 9, temperatures are maximized for the pseudoplastic case ($n = 0.5$), whereas in Fig. 6 they are greatest for the Newtonian fluid. Clearly in Fig. 6, since Brownian motion effect is being varied, this parameter has a complex interaction with the thermal field, which alters the familiar response computed in other figures. Both an increase in Nt and Nb result in a substantial accentuation in temperatures (Fig. 8, 9 respectively). This will therefore be accompanied with a significant increase in thermal boundary layer thickness. Thermophoresis relates to increasing nanoparticle deposition on the sheet surface in the direction of a decreasing temperature gradient. As such, the nanofluid temperature is elevated by this enhancement in particle migration, a trend also observed by numerous experimental studies including Eastman et al. [37] and many theoretical simulations including Kuznetsov and Nield [27]. Within the framework of the Kuznetsov–Nield theory, a nanofluid behaves significantly more as a viscous fluid rather than the conventional solid-fluid mixtures in which relatively larger particles with micrometer or millimetre orders are suspended. Nevertheless, since the nanofluid is a two-phase fluid in nature and has some common features with solid-fluid mixtures, it does exhibit similar shear characteristics. The enhanced heat transfer by the nanofluid may result from either the fact that the suspended particles increase the thermal conductivity of the two-phase mixture or owing to chaotic movement of ultrafine particles accelerating energy exchange process in the fluid. However much needs to be resolved in elucidating more explicitly the exact mechanisms for the contribution of suspended particles to thermal enhancement, and in this regard the micro-structure of the nanofluid (whether Newtonian or non-Newtonian) may provide a more robust fluid dynamical frame work. Indeed this has been explored by Gorla and Kumari [38] with the Eringen micropolar model, and most recently by Be'g [39] using the Eringen micro-stretch model with greater degrees of freedom of micro-elements. These studies have revealed that the gyratory motions of micro-elements containing the nanoparticles exert a significant influence on thermal transport, and capture features which are basically not realizable even in rheological nanofluid models which neglect microstructural properties. Although the present power-law model would indicate that thermal conductivity is boosted in the nanofluid, it is not possible to analyze whether the spin of nanoparticles is also a contributory factor. It is envisaged therefore that the ‘‘microstructural’’ rheological models of Eringen [40] which have been reviewed comprehensively in computational micropolar transport modeling by Be'g et al. [41] will also be deployed for stretching sheet magneto-nanofluid dynamics as explored in the near future. Figure 9 demonstrates that a rise in Prandtl number (Pr) effectively suppresses the nanofluid temperatures. Temperature is however for both Newtonian and non-Newtonian nanofluids, reduced markedly with an increase in Pr . Pr defines the ratio of momentum diffusivity to thermal diffusivity for a given nanofluid. With lower Pr nanofluids, heat diffuses faster than momentum (the energy diffusion rate exceeds the viscous diffusion rate) and vice versa for higher Pr fluids. With an increase in Pr , temperatures will therefore fall, i.e., the nanofluid boundary layer regime will be cooled as observed in Fig. 10. Larger Prandtl values correspond to a thinner thermal boundary layer thickness and more uniform temperature distributions across the boundary layer. Smaller Pr nanofluids possess higher thermal conductivities so that heat can diffuse away from the vertical plate faster than for higher Pr fluids (low Pr fluids correspond to thicker boundary layers). We finally note that for the Newtonian case with maximum Pr ($=6.8$) temperature plummets very sharply from the sheet surface and assumes very low values very quickly. At the other extreme, with the lowest value of Pr ($=0.72$) a very gentle decay. Figs. 11&12 depicts the response of temperature profiles, again for both pseudoplastic ($n=0.5$) and Newtonian ($n=1$) fluids, for a variation in permeability parameter, temperature dependent slip parameter. It is found that the temperature increases with increasing the permeability parameter and the temperature decreases with a raising the thermal slip parameter these similar finding are observed in Mutlag et al. [20] in the case of Newtonian fluid flow ($n=1$).

Figure 13-15 depicts the variation of nanoparticle concentration profiles for Newtonian and pseudoplastic nanofluids, with different values of the momentum slip (a), lateral mass flux (S) and thermophoresis (Nt) parameters. In all the figures greater concentration magnitudes are attained with pseudoplastic fluids than Newtonian fluids. The concentration profiles increases with increasing wall slip and thermophoresis and furthermore are also enhanced with greater injection at the sheet surface. Enhanced migration of suspended nanoparticles via the mechanisms of thermophoresis, increases energy exchange rates in the fluid and simultaneously assists in nanoparticle diffusion, leading to greater values of concentration profiles. The dispersion of nanoparticles will not only successfully heat the boundary layer and augment heat transfer rate from the nanofluid to the wall, but will also enhance concentration (species) boundary layer thicknesses.

Figs. 16&17, illustrates the nanoparticle concentration distributions with a variation in Brownian motion parameter (Nb) and Lewis number (Le), again for both Newtonian and pseudoplastic nanofluids. The general pattern observed in most of the computations described in earlier figures is confirmed in Fig. 16, 17,

namely, that pseudoplastic fluids achieve greater concentration magnitudes relative to Newtonian nanofluids. As indicated in many studies including Kuznetsov and Nield [27] for Newtonian nanofluids, Sheu [42] for viscoelastic nanofluids and Uddin et al. [43] for power-law nanofluids, an increase in Brownian motion parameter effectively depresses nanoparticle concentrations in the nanofluid regime. This is attributable to the enhanced mass transfer to the sheet wall from the main body of the nanofluid (boundary layer) with increasing Brownian motion. Among others, Rana et al. [32,34] have demonstrated that the Brownian motion of nanoparticles achieves thermal conductivity enhancement either by way of a direct effect owing to nanoparticles that transport heat or alternatively via an indirect contribution due to micro-convection of fluid surrounding individual nanoparticles. For larger nanoparticles (and in the present study all nanoparticles in the nanofluid possess consistent sizes) Brownian motion is weakened so that Nb has lower values this aids in species diffusion from the wall to the nanofluid and elevates nanoparticle concentration values. The exact opposite is manifested with higher Nb values. As anticipated the Brownian motion parameter causes a substantial modification in nanoparticle species distributions throughout the boundary layer regime. An even more dramatic effect is induced on the nanoparticle concentrations, via an increase in the Lewis number (Fig. 17). This dimensionless number signifies the ratio of thermal diffusivity to mass diffusivity in the nanofluid. It is used to characterize fluid flows where there is simultaneous heat and mass transfer by convection. Le also expresses the ratio of the Schmidt number to the Prandtl number. For $Le = 1$, both heat and nanoparticle species will diffuse at the same rate. For $Le < 1$, heat will diffuse more slowly than nanoparticle species and vice versa for $Le > 1$. For the cases examined here, $Le \geq 1$, i.e., thermal diffusion rate substantially exceeds the mass fraction (species) diffusion rate. Inspection of Fig. 17 shows that nanoparticle concentration is clearly also suppressed with an increase in Le . Finally Fig. 18-21, illustrates the nanoparticle concentration distributions with a variation in magnetic parameter (M), permeability parameter (K), thermal slip parameter (b) and chemical reaction parameter (kr), again for both Newtonian and pseudoplastic nanofluids. It is noticed that the nanoparticle concentration increases with a raising the magnetic parameter and permeability parameter (fig 18&19) and also noticed that nanoparticle concentration decreases with an increasing the thermal slip parameter and chemical reaction parameter.

Figure 22 shows the effects of S and K on skin friction. From Figure 22 it is seen that the skin friction decreases with an increase S or K . The effect of Nt and Nb on local Nusselt number is shown in fig.23. It is found that the local Nusselt number reduces with an increase in the parameters Nt and Nb . The variations of Nt and Nb on local Nusselt number are shown in fig.24. It is observed that the local Nusselt number decrease with an increasing the parameter Nt whereas local Nusselt number increases with an raising Nb .

V. Conclusions

In the present prater, the two-dimensional magnetohydrodynamic boundary layer flow of non-Newtonian power-law nanofluids past a porous stretching sheet with linear hydrodynamic slip boundary condition in the presence of chemical reaction and temperature dependent slip boundary condition. The governing equations are approximated to a system of non-linear ordinary differential equations by similarity transformation. Numerical calculations are carried out for various values of the dimensionless parameters of the problem. It has been found that

1. Increasing momentum slip parameter decelerates the boundary layer flow (reduces velocities) whereas it generally strongly increases temperatures and nanoparticle concentration values.
2. With increasing wall injection, velocity, temperature and concentration are generally enhanced with the converse behaviour observed with increasing wall suction.
3. Increasing permeability parameter markedly decelerates the flow, increases momentum boundary layer thickness and moreover induces a noteworthy elevation in temperatures as well as nanoparticle concentration and thermal boundary layer thickness.
4. Increasing thermophoresis parameter boosts both the temperatures and nanoparticle concentration magnitudes throughout the boundary layer regime.
5. Increasing Brownian motion parameter enhances temperatures strongly whereas it markedly depresses nanoparticle concentration values.
6. Increasing thermal slip parameter reduces both the temperatures and nanoparticle concentration magnitudes throughout the boundary layer regime.
7. Increasing Lewis numbers significantly stifles nanoparticle concentration values.
8. Generally the flow is accelerated, temperatures increased and nanoparticle concentrations boosted for pseudoplastic nanofluids with the converse for Newtonian nanofluids.

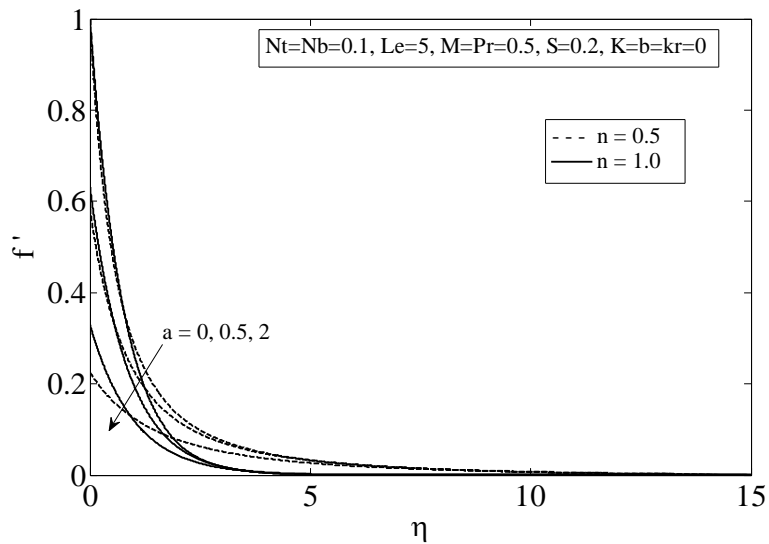


Fig.1 Velocity for different values of a and n

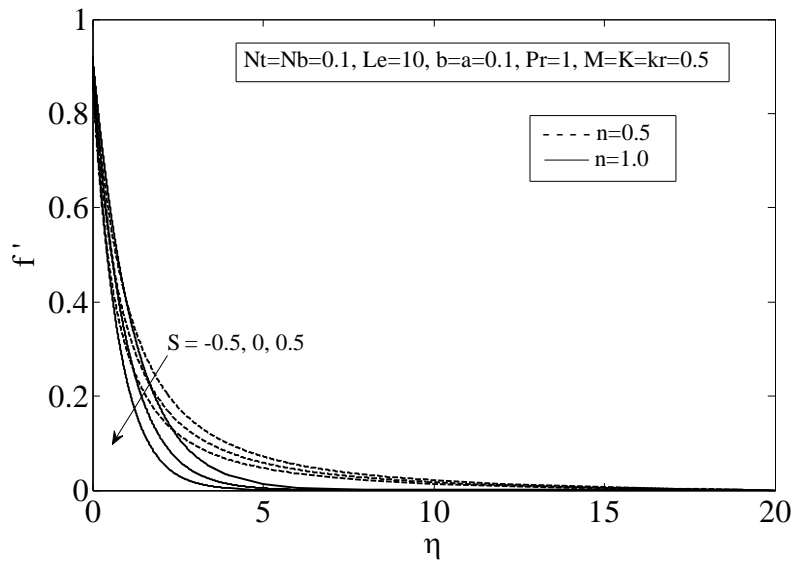


Fig.2 Velocity for different values of S and n

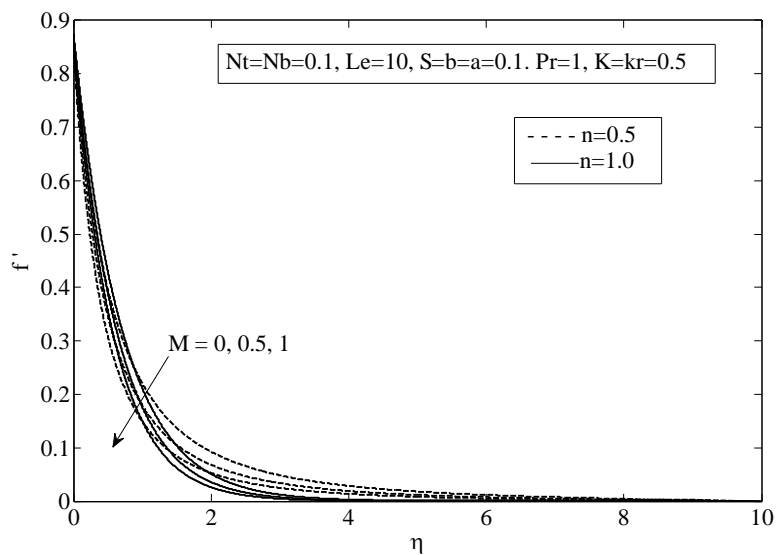


Fig.3 Velocity for different values of M and n

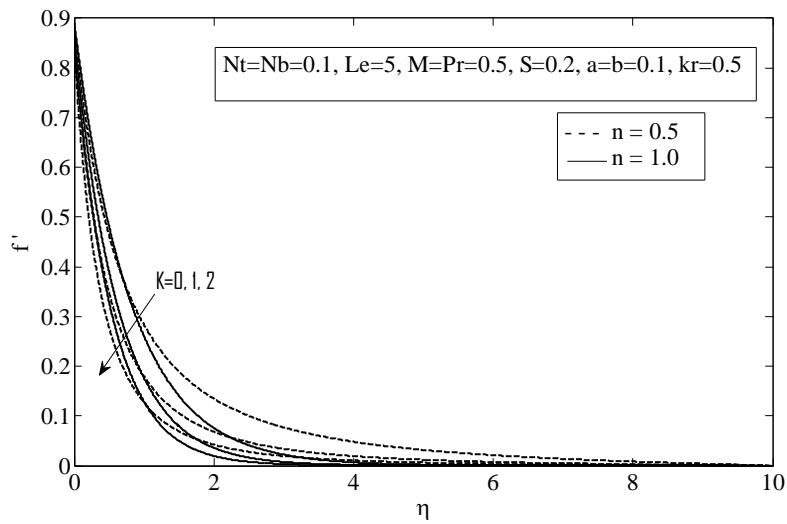


Fig.4 Velocity for different values of K and n

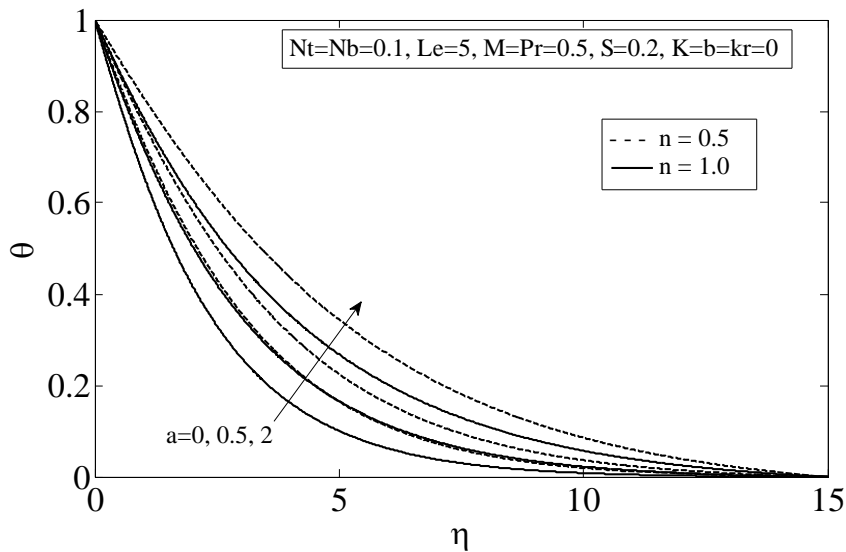


Fig.5 Temperature for different values of a and n

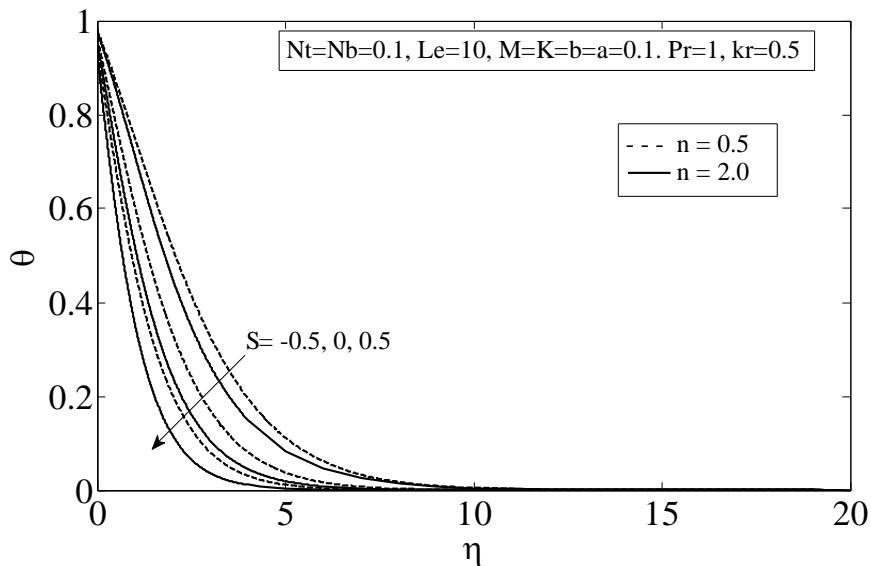


Fig.6 Temperature for different values of S and n

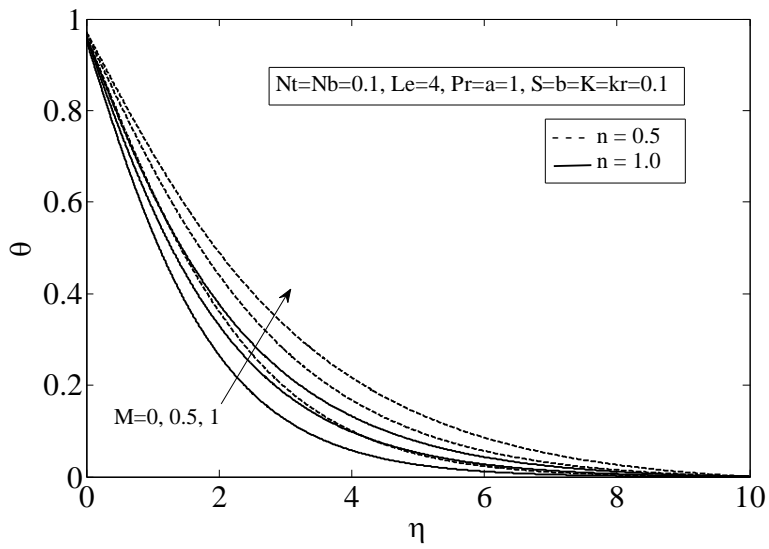


Fig.7 Temperature for different values of M and n

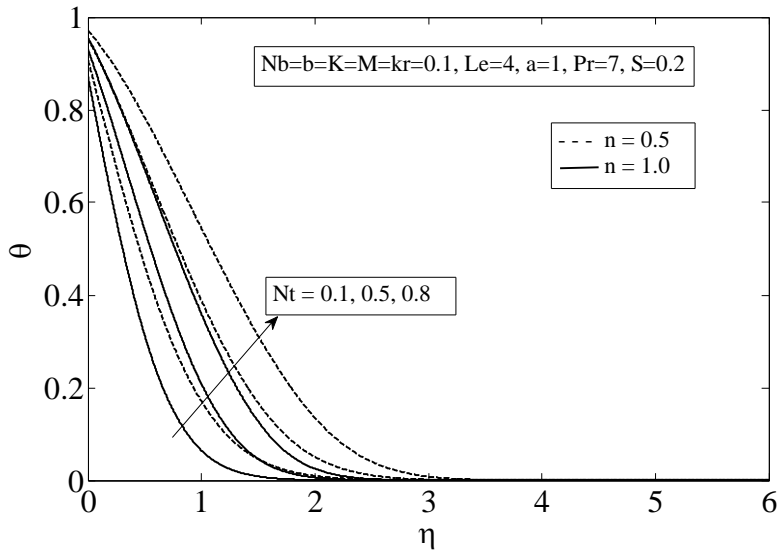


Fig.8 Temperature for different values of Nt and n

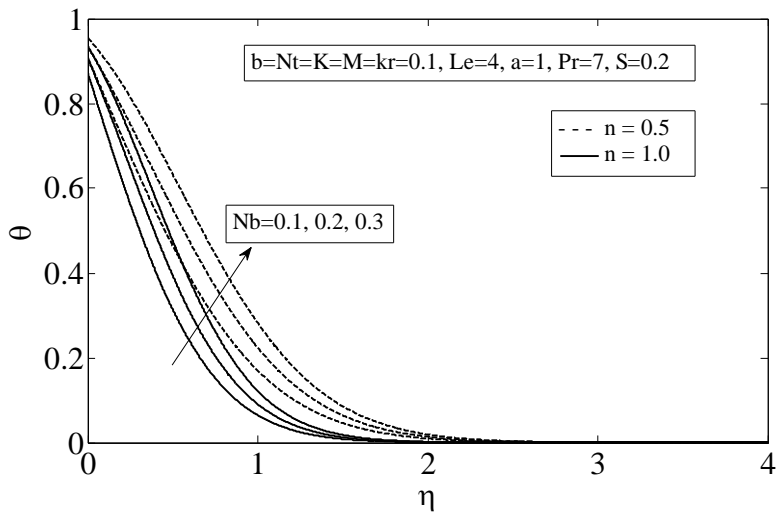


Fig.9 Temperature for different values of Nb and n

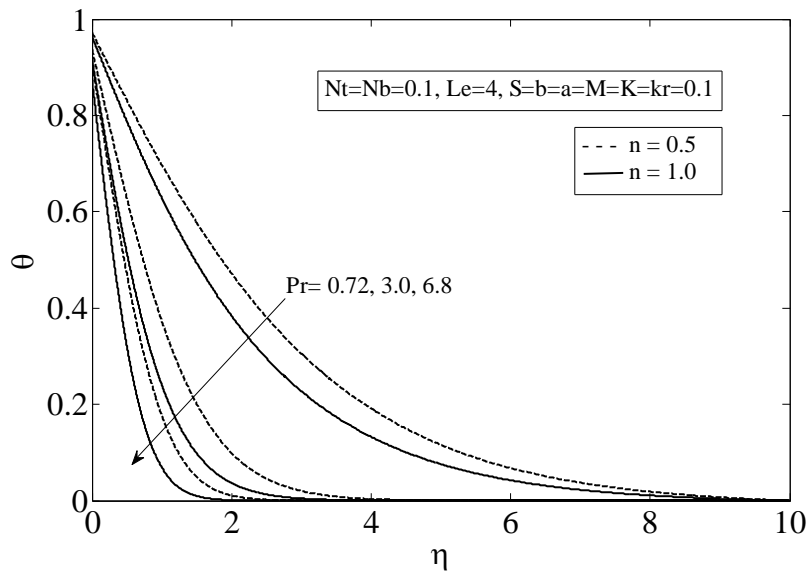


Fig.10 Temperature for different values of Pr and n

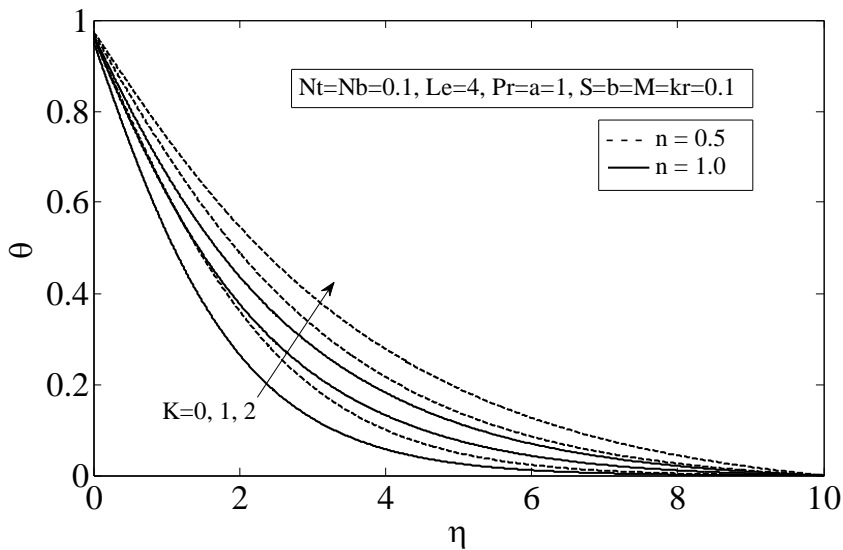


Fig.11 Temperature for different values of K and n

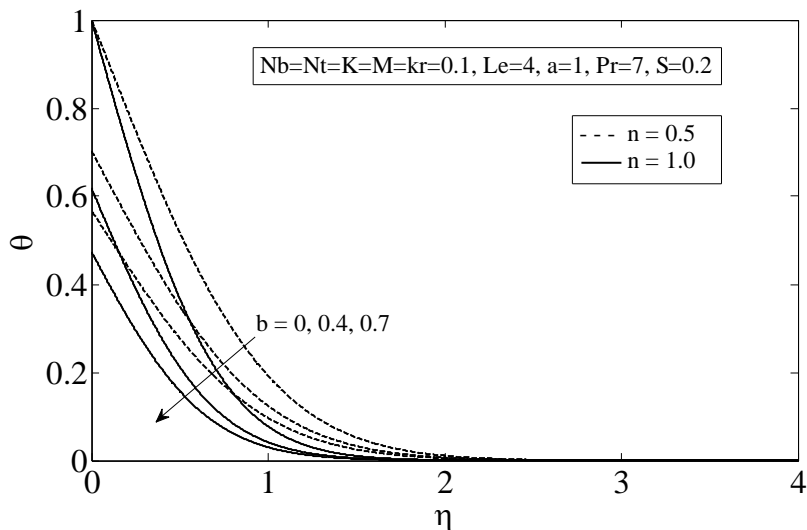


Fig.12 Temperature for different values of b and n

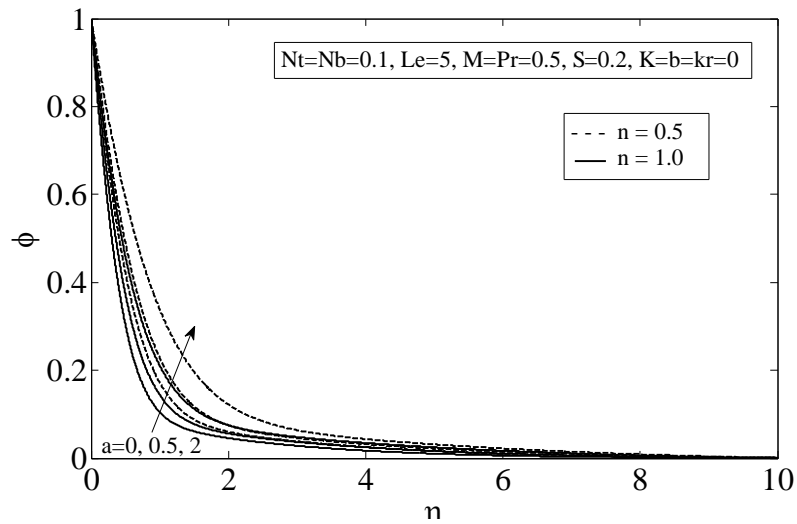


Fig.13 Concentration for different values of a and n

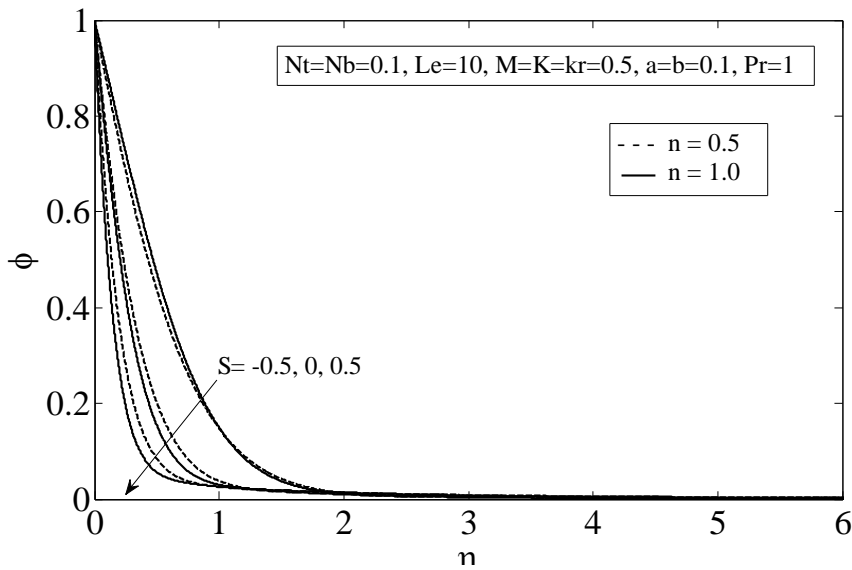


Fig.14 Concentration for different values of S and n

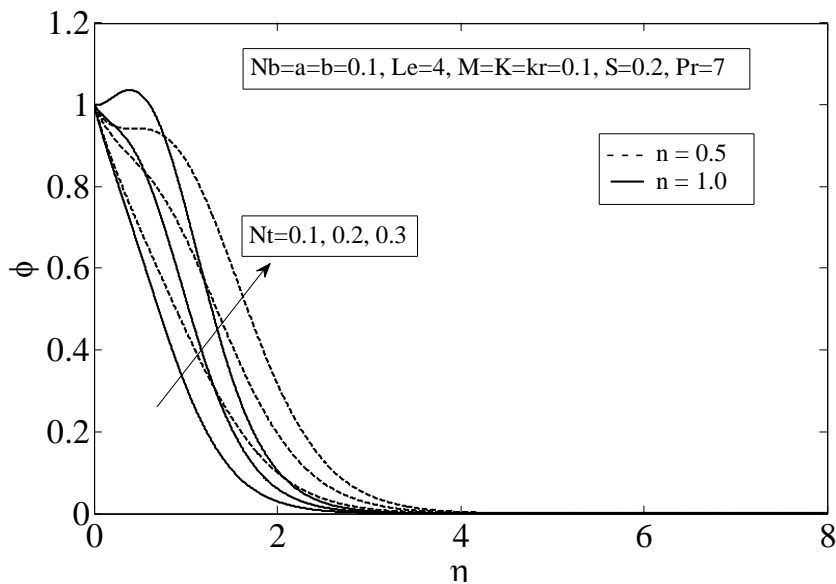


Fig.15 Concentration for different values of Nt and n

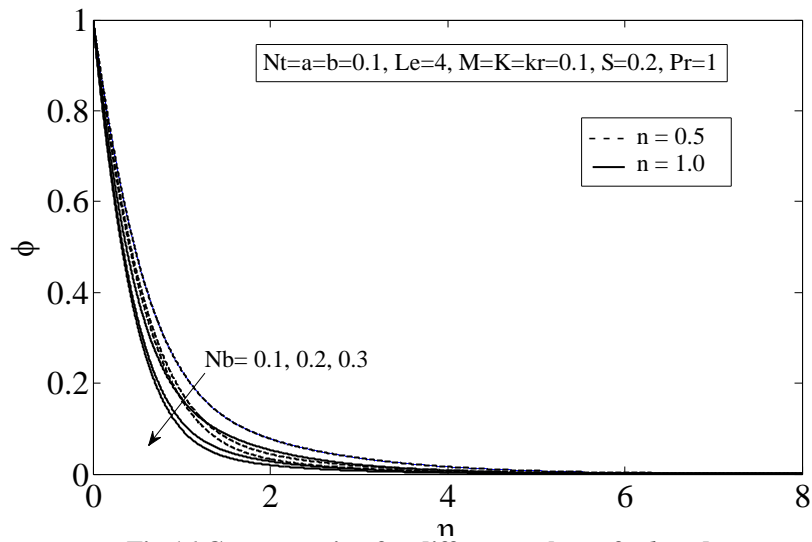


Fig.16 Concentration for different values of Nb and n

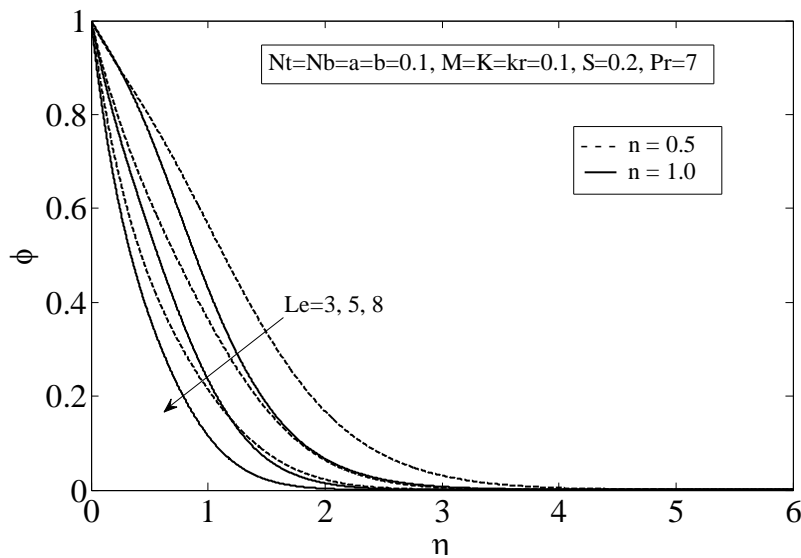


Fig.17 Concentration for different values of Le and n

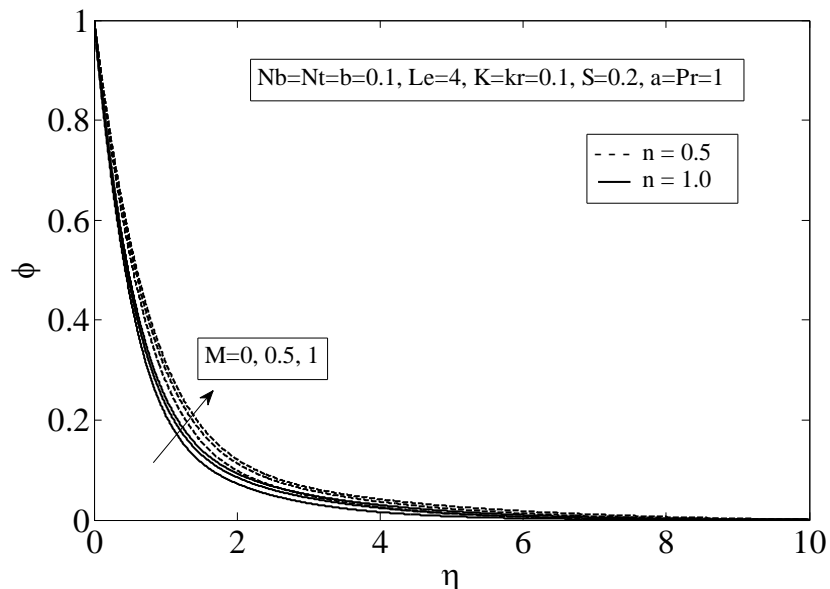


Fig.18 Concentration for different values of M and n

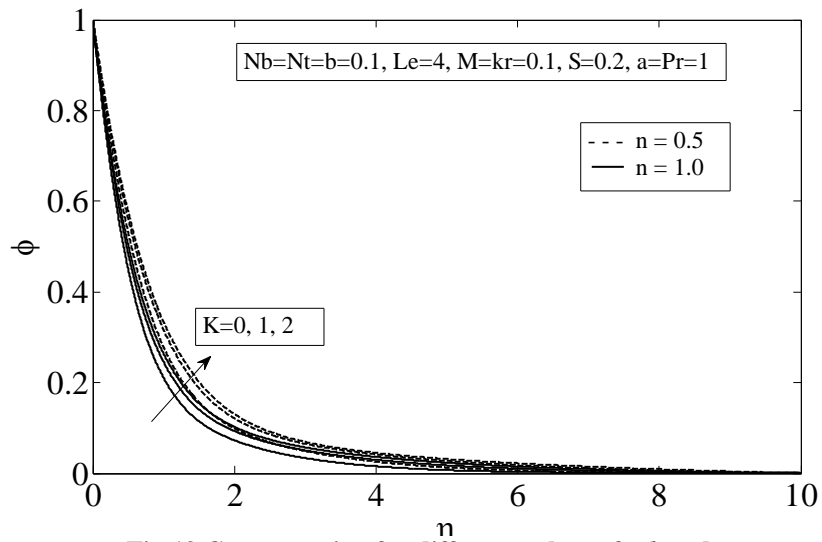


Fig.19 Concentration for different values of Nb and n

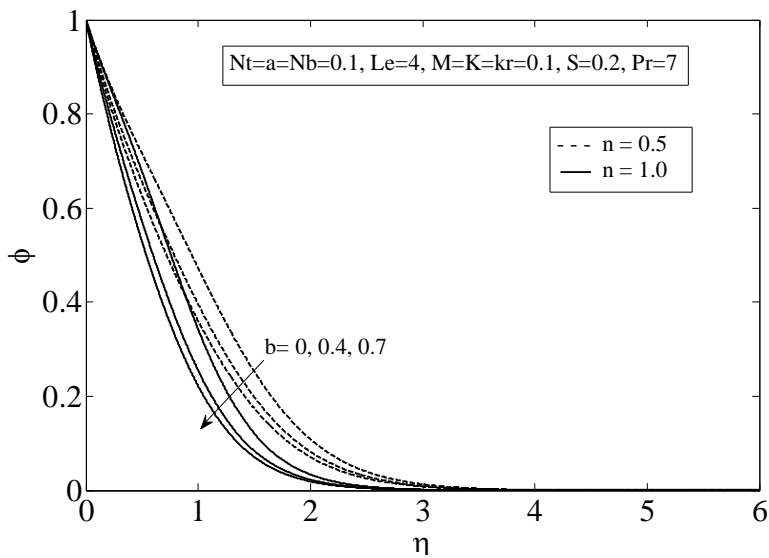


Fig.20 Concentration for different values of b and n

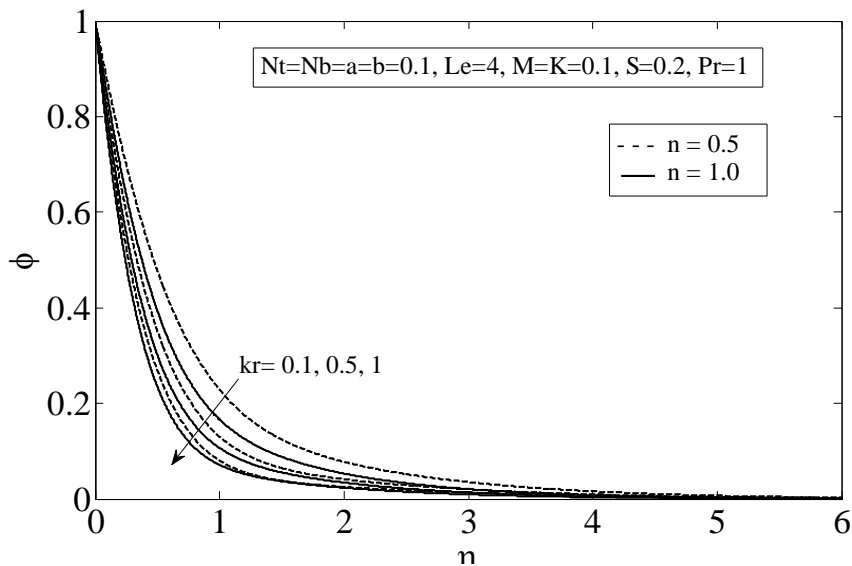


Fig.21 Concentration for different values of kr and n

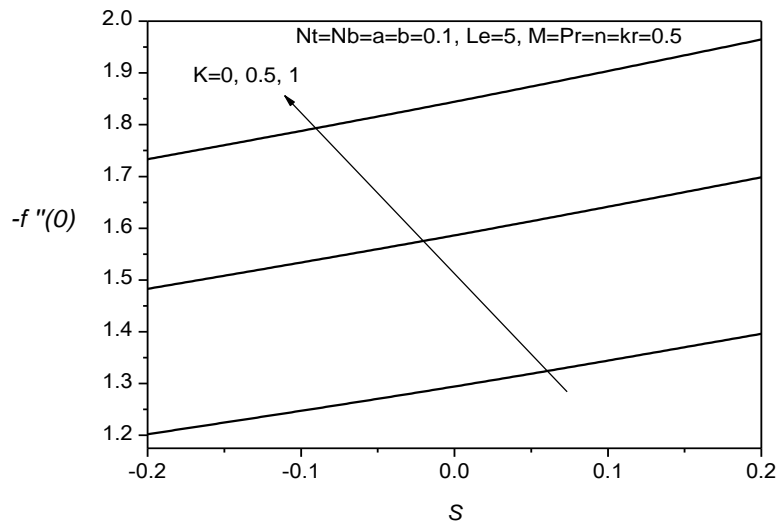


Fig.22 Local Skin-friction for different values of S and K

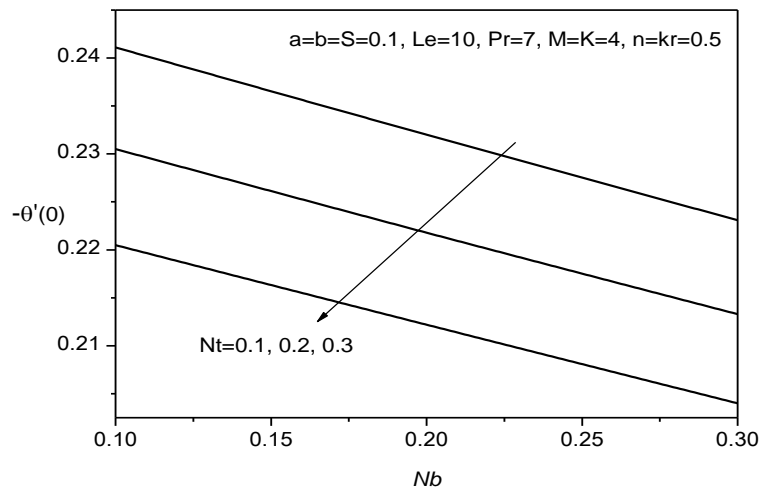


Fig.23 Local Nusselt number for different values of Nb and Nt

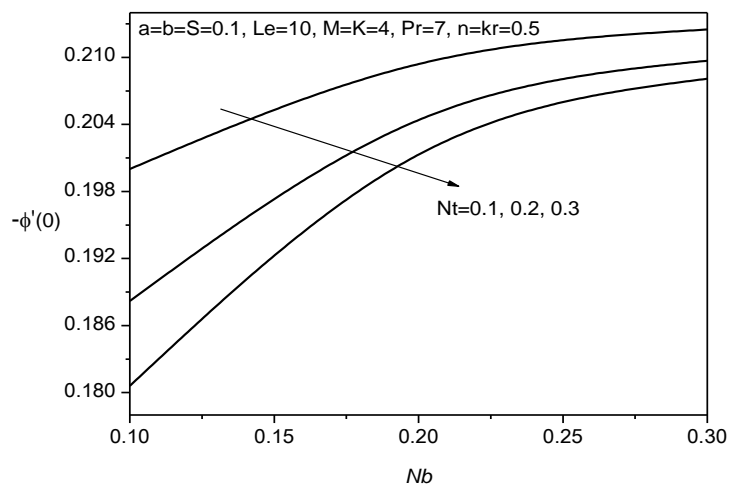


Fig.24 Local Sherwood number for different values of Nb and Nt

Table.1 Comparison for the values of $-f''(0)$ for $M=K=S=0$ and various values of n

n	$-f''(0)$			
	Present results	Uddin et al. [15]	Xu and Liao [26]	Andersson and Bech [21]
0.4	1.274491	1.27306	-	1.273
0.6	1.096059	1.09644	-	1.096
0.8	1.028470	1.02883	1.02853	1.029
1.0	1.000000	1.00000	1.00000	1.000
1.5	0.980987	1.19281	0.98237	0.981

Table.2 Comparison for the values of $-f''(0)$ for $K=S=0$ and various values of n and M

n	$-f''(0)$											
	Present results				Uddin et al. [15]				Andersson and Bech [21]			
	M=0.5	M=1	M=1.5	M=2	M=0.5	M=1	M=1.5	M=2	M=0.5	M=1	M=1.5	M=2
0.4	1.810994	2.283844	2.718692	3.126658	1.812	1.777	2.719	3.127	1.811	2.284	2.719	3.127
0.6	1.462878	1.777027	2.059897	2.320780	1.463	1.544	2.060	2.321	1.463	1.777	2.060	2.321
0.8	1.307859	1.544114	1.754012	1.945332	1.308	1.414	1.754	1.945	1.309	1.544	1.754	1.945
1.0	1.224745	1.414214	1.581139	1.732051	1.225	1.384	1.581	1.732	1.225	1.414	1.581	1.732
1.2	1.174989	1.333013	1.471504	1.595994	1.252	1.280	1.507	1.621	1.175	1.333	1.472	1.596
1.5	1.130779	1.257081	1.367223	1.465658	1.168	2.284	1.381	1.475	1.131	1.257	1.367	1.466

Table.3 Comparison for the values of $-\theta'(0)$ for $n=1, Nt=Nb=b=0$ and various values of Pr

Pr	$-\theta'(0)$				
	Present results	Uddin et al. [15]	Ishak [31]	Chen [30]	Grubka and Bobba [29]
0.01	0.054647	0.128936	0.0099	0.0099	0.0099
0.72	0.463145	0.465014	0.4631	0.46315	0.46315
1	0.581977	0.582228	0.5820	0.58199	0.58199
3	1.165246	1.165217	1.1652	1.16523	1.16523
10	2.308004	2.307984	2.3080	2.30796	2.30796
100	7.765652	7.765637	7.7657	7.76536	7.76536

References

- [1]. Choi, S., Enhancing thermal conductivity of fluids with nanoparticles, in: D.A. Siginer, H.P.
- [2]. Masuda, H., Ebata, A., Teramae, K., Hishinuma, N., (1993), Alteration of thermal conductivity and viscosity of liquid by dispersing ultra-fine particles, *NetsuBussei (Japan)*, Vol.7, No.4, pp.227–233.
- [3]. Pearson, J. R. A., Tardy, P. M. J., (2002), Models for flow of non-Newtonian and complex fluids through porous media, *J Non Newton Fluid Mech*, Vol.102, pp.447–473.
- [4]. Ellahi R, Afza, S., (2009), Effects of variable viscosity in a third grade fluid with porous medium: an analytic solution, *Commun Nonlinear Sci Numer Simul.*, Vol.14(5), pp.2056–2072.
- [5]. Ellahi, R., (2009), Effects of the slip boundary condition on non-Newtonian flows in a channel, *Commun Nonlinear Sci Numer Simul.*, Vol.144, pp.1377–1384.
- [6]. Rama Subba Reddy Gorla and Mahesh Kumari, (2012), Mixed Convection Flow of a Non-Newtonian Nanofluid Over a Non-Linearly Stretching Sheet, *Journal of Nanofluids*, Vol. 1, pp. 186–195.
- [7]. Crane, L. J., (1970), Flow past a stretching plate, *Journal of Applied Mathematics and Physics*, Vol. 21, No. 4, pp. 645–647.
- [8]. Wang, C. Y., (2009), Analysis of viscous flow due to a stretching sheet with surface slip and suction, *Nonlinear Analysis: Real World Applications*, Vol. 10, No. 1, pp. 375-380.
- [9]. Qasim, M., Khan, Z.H., Khan, W.A., and Ali Shah, I., (2014), MHD Boundary Layer Slip Flow and Heat Transfer of Ferrofluid along a Stretching Cylinder with Prescribed Heat Flux, *PLoS ONE* 9(1): e83930. doi:10.1371/journal.pone.0083930.
- [10]. AbdEl-Gaied, S. M., and Hamad, M. A. A., (2013), MHD Forced Convection Laminar Boundary Layer Flow of Alumina-Water Nanofluid over a Moving Permeable Flat Plate with Convective Surface Boundary Condition, *Hindawi Publishing Corporation, Journal of Applied Mathematics*, Volume 2013, Article ID 403210, 8 pages
- [11]. Nandy, S. K., and Mahapatra, T. R., (2013), Effects of slip and heat generation/absorption on MHD stagnation flow of nanofluid past a stretching/shrinking surface with convective boundary conditions, *International Journal of Heat and Mass Transfer*, Vol. 64, pp. 1091-1100.
- [12]. Eldabe, N. T., Elbashareshy, E. M. A., Elsaid, E. M., (2013), Effects of Magnetic Field and Heat Generation on Viscous Flow and Heat Transfer over a Nonlinearly Stretching Surface in a Nanofluid, *International Journal of Applied Mathematics*, ISSN:2051-5227, Vol.28, Issue.1
- [13]. Krishnendu Bhattacharyya, Swati Mukhopadhyay, and Layek, G. C., (2011), MHD Boundary Layer Slip Flow and Heat Transfer over a Flat Plate, *Chin. Phys. Lett.*, Vol. 28, No. 2.
- [14]. Santosh Chaudhary and Pradeep Kumar, (2013), MHD Slip Flow past a Shrinking Sheet, *Applied Mathematics*, Vol. 4, pp.574-581
- [15]. Uddin, M. J., M. Ferdows, O. Anwar Be'g, Group analysis and numerical computation of magneto-convective non-Newtonian nanofluid slip flow from a permeable stretching sheet, *Appl Nanosci.*, DOI 10.1007/s13204-013-0274-1
- [16]. Mierzwiczak, M. & Kołodziej, J.A. 2011. The determination temperature-dependent thermal conductivity as inverse steady heat conduction problem. *International Journal of Heat and Mass Transfer* 54: 790-796.
- [17]. Abel, M.S., Siddheshwar, P.G. & Mahesha, N. 2009. Effects of thermal buoyancy and variable thermal conductivity on the MHD flow and heat transfer in a power-law fluid past a vertical stretching sheet in the presence of a non-uniform heat source. *International Journal of Non-Linear Mechanics* 44: 1-12.
- [18]. Ahmad, N., Siddiqui, Z.U. & Mishra, M.K. 2010. Boundary layer flow and heat transfer past a stretching plate with variable thermal conductivity. *International Journal of Non-Linear Mechanics* 45: 306-309.

- [19]. Shang, D. 2010. Theory of Heat Transfer with Forced Convection Film Flows. Chapter 7. New York: Springer.
- [20]. Mutlag, A.A., Md. JashimUddin, M.A.A. Hamad & Ahmad Izani Ismail, Heat Transfer Analysis for Falkner-Skan Boundary Layer Flow Past a Stationary Wedge with Slips Boundary Conditions Considering Temperature-dependent Thermal Conductivity, Sains Malaysiana 42(6)(2013): 855–862.
- [21]. Andersson HI, Bech KH (1992) Magneto hydrodynamic flow of a power law fluid over a stretching sheet. Int J Non-Linear Mech 27:929–936
- [22]. Makinde OD, Aziz A (2011) Boundary layer flow of a nanofluid past a stretching sheet with a convective boundary condition. Int J Therm Sci 50:1326–1332
- [23]. Hansen AG (1964) Similarity analysis of boundary layer problems in engineering. Prentice Hall Englewood Cliffs, New Jersey.
- [24]. Shang D (2010) Theory of heat transfer with forced convection film flows (Heat and Mass Transfer). Springer, Berlin.
- [25]. Noghrehabadi A, Pourrajab R, Ghalambaz M (2012) Effect of partial slip boundary condition on the flow and heat transfer of nanofluids past stretching sheet prescribed constant wall temperature. Int J Therm Sci 54:253–261.
- [26]. Xu H, Liao S-J (2009) Laminar flow and heat transfer in the boundary layer of non-Newtonian fluids over a stretching flat sheet. Comp Maths Applics 57:1425–1431.
- [27]. Kuznetsov AV, Nield DA (2010) Natural convective boundary-layer flow of a nanofluid past a vertical plate. Int J Therm Sci 49:243–247.
- [28]. Shampine, L. F. and Kierzenka, J. (2000), “Solving boundary value problems for ordinary differential equations in MATLAB with bvp4c,” Tutorial Notes.
- [29]. Grubka LJ, Bobba KM (1985) Heat transfer characteristics of a continuous, stretching surface with variable temperature. ASME J Heat Transf 107:248–250
- [30]. Chen CH (1998) Laminar mixed convection adjacent to vertical, continuously stretching sheets. Heat Mass Transf 33:471–476
- [31]. Ishak A (2010) Thermal boundary layer flow over a stretching sheet in a micropolar fluid with radiation effect. Meccanica 45:367–373
- [32]. Rana P, Bhargava R, Be'g OA (2013a) Finite element modeling of conjugate mixed convection flow of Al₂O₃-water nanofluid from an inclined slender hollow cylinder. Physica Scripta-Proc Royal Swedish Acad Sci 87:1–16.
- [33]. Be'g OA, Zueco J, Lopez-Ochoa LM (2011a) Network numerical analysis of optically thick hydromagnetic slip flow from a porous spinning disk with radiation flux, variable thermophysical properties and surface injection effects. Chem Eng Commun 198:360–384
- [34]. Rana P, Bhargava R, Be'g O Anwar (2013b) Finite element simulation of unsteady MHD transport phenomena on a stretching sheet in a rotating nanofluid. Proc IMechE Part N: J Nanoeng Nanosyst. doi:10.1177/1740349912463312
- [35]. Ferdows M, Khan MS, Be'g OA, Azad MK, Alam MM (2013) Numerical study of transient magnetohydrodynamic radiative free convection nanofluid flow from a stretching permeable surface. Proc IMechE Part E: J Process Mech Eng. doi:10.1177/0954408913493406
- [36]. Crainic N, Marques AT, Bica D (2003) The usage of nanomagnetic fluids and magnetic field to enhance the production of composite made by RTM-MNF. In: 7th International Conference. Frontiers- Polymers/Advanced Materials. Romania, pp 10–15.
- [37]. Eastman JA, Phillpot SR, Choi SUS, Keblinski P (2004) Nanofluids for thermal transport. Ann Rev Mat Res 34:219
- [38]. Gorla RSR, Kumari M (2012) Mixed convection flow of a non-Newtonian nanofluid over a non-linearly stretching sheet. J Nanofluids 1:186–195
- [39]. Be'g OA, Prasad VR, Vasu B (2013a) Numerical study of mixed bio convection in porous media saturated with nanofluid containing oxytactic micro-organisms. J Mech Med Biol. doi:10. 1142/S021951941350067X
- [40]. Eringen AC (2001) Microcontinuum field theories-II: fluent media. Springer, USA
- [41]. Be'g OA, Bhargava R, Rashidi MM (2011c) Numerical simulation in micropolar fluid dynamics. Lambert Academic Press, Saarbrücken
- [42]. Sheu LJ (2011) Thermal instability in a porous medium layer saturated with a viscoelastic nanofluid. Transp Porous Media 88:461–477
- [43]. Uddin MJ, Khan WA, Ismail AIM (2013b) Free convective flow of non-Newtonian nanofluids in porous media with gyrotactic microorganisms. AIAA J Thermophys Heat Transfer 27:326–333.